RESSALVA

Atendendo solicitação do(a) autor(a), o texto completo desta tese será disponibilizado somente a partir de 28/06/2020.

UNIVERSIDADE ESTADUAL PAULISTA
CAMPUS ARARAQUARA
PROGRAMA DE PÓS-GRADUAÇÃO EM QUÍMICA

Silver (Ag) nanoclusters and lanthanides (Er^{3+}, Pr^{3+}, Yb^{3+}) ions functionalized glassy materials for light sources, luminescent layers for silicon solar cell and waveguide application

TARCIO DE CASTRO SILVA

PhD Thesis
2018

TARCIO DE CASTRO SILVA

Silver (Ag) nanoclusters and lanthanides (Er^{3+}, Pr^{3+}, Yb^{3+}) ions functionalized glassy materials for light sources, luminescent layers for silicon solar cell and waveguide application

Thesis submitted to the Institut of Chemistry, São Paulo State University (Araraquara), in partial fulfillment of the requirements for the degree of Doctor in Chemistry.

Araraquara
2018

FICHA CATALOGRÁFICA

Silva, Tarcio de Castro
S586s Silver (Ag) nanoclusters and lanthanides (Er^{3+}, Pr^{3+}, Yb^{3+}) ions functionalized glassy materials for light sources, luminescent layers for silicon solar cell and waveguides application / Tarcio de Castro Silva. – Araraquara : [s.n], 2018
134 f. : il.

Thesis (doctor) – Universidade Estadual Paulista, Instituto de Química
Advisor: Sidney José Ribeiro

1. Spectral analysis. 2. Optical glasses. 3. Rare earth metals. 4. Nanostructured materials. 5. Photonic. I. Título.

Elaboração: Seção Técnica de Aquisição e Tratamento da Informação
Biblioteca do Instituto de Química, Unesp, Câmpus de Araraquara

UNIVERSIDADE ESTADUAL PAULISTA

Câmpus de Araraquara

CERTIFICADO DE APROVAÇÃO

TÍTULO DA TESE: "Silver (Ag) nanoclusters and lanthanides (Er^{3+}, Pr^{3+}, Yb^{3+}) ions functionalized glassy materials for light sources, luminescent layers for silicon solar cell and waveguide application"

AUTOR: TARCIO DE CASTRO SILVA
ORIENTADOR: SIDNEY JOSE LIMA RIBEIRO

Aprovado como parte das exigências para obtenção do Título de Doutor em QUÍMICA, pela Comissão Examinadora:

Prof. Dr. SIDNEY JOSE LIMA RIBEIRO
Departamento de Química Geral e Inorgânica / Instituto de Química - UNESP - Araraquara

Prof. Dr. MARCELO NALIN
Departamento de Química Geral e Inorgânica / Instituto de Química - UNESP - Araraquara

Prof. Dr. HERMI FELINTO DE BRITO
Departamento de Química Fundamental / Instituto de Química - USP - São Paulo

Profª. Drª. ROGÉRIA ROCHA GONÇALVES
Departamento de Química / Faculdade de Filosofia Ciências e Letras - USP - Ribeirão Preto

VÍDEOCONFERÊNCIA
Prof. Dr. THIERRY CARDINAL
Chimie et Photonique des Matériaux Oxydes et Fluorures / Institut de Chimie de la Matière Condensée de Bordeaux

Araraquara, 28 de junho de 2018

UNIVERSIDADE ESTADUAL PAULISTA

Câmpus de Araraquara

CERTIFICADO DE APROVAÇÃO

TÍTULO DA TESE: "Silver (Ag) nanoclusters and lanthanides (Er^{3+}, Pr^{3+}, Yb^{3+}) ions functionalized glassy materials for light sources, luminescent layers for silicon solar cell and waveguide application"

AUTOR: TARCIO DE CASTRO SILVA
ORIENTADOR: SIDNEY JOSE LIMA RIBEIRO

Aprovado como parte das exigências para obtenção do Título de Doutor em QUÍMICA, pela Comissão Examinadora:

Prof. Dr. SIDNEY JOSE LIMA RIBEIRO
Departamento de Química Geral e Inorgânica / Instituto de Química - UNESP - Araraquara

Prof. Dr. MARCELO NALIN
Departamento de Química Geral e Inorgânica / Instituto de Química - UNESP - Araraquara

Prof. Dr. HERMI FELINTO DE BRITO
Departamento de Química Fundamental / Instituto de Química - USP - São Paulo

Profª. Drª. ROGÉRIA ROCHA GONÇALVES
Departamento de Química / Faculdade de Filosofia Ciências e Letras - USP - Ribeirão Preto

Prof. Dr. THIERRY CARDINAL
Chimie et Photonique des Matériaux Oxydes et Fluorures / Institut de Chimie de la Matière Condensée de Bordeaux

Araraquara, 28 de junho de 2018

CURRICULUM VITAE

IDENTIFICATION

Full name: Tarcio de Castro Silva

Nationality: Brazilian

Name in scientific citations: Silva, T. C.; Silva, Tarcio de Castro.

Professional address: Rua Francisco Degni n° 55, Bairro Quitandinha, Araraquara – SP, Brasil.

E-mail contact: tarcioquimica@gmail.com

EDUCATION

Graduation: Universidade Federal de Goiás (UFG); Bachelor's degree in Chemistry/(2007-2011).

Master: Universidade Federal de Goiás (UFG); Advisor: Jesiel Freitas Carvalho; co-advisor: Lauro Queiroz June Maia; (2011-2013).

PhD: Universidade Paulista "Júlio de Mesquita Filho" (UNESP)/ Campus Araraquara. São Paulo – Brasil. Advisor: Sidney José Lima Ribeiro; (2014-2018).

PUBLICATIONS IN SCIENTIFIC JOURNALS

SILVA, T. C.; MANZANI, Danilo; RIBEIRO, S. J. L. Up-conversion mechanisms in Er^{3+}-doped fluoroindate glasses under 1550 nm excitation for enhancing photocurrent of crystalline silicon solar cell. **Journal of Luminescence**, v. 200, p. 260-264, 2018.

FARES, H.; CASTRO, T.; ORIVES, J. R.; FRANCO, D. F.; Nalim, M. White light and multicolor emission tuning in Ag nanocluster doped fluorophosphate glasses. **RSC Advances**, v. 7, p. 44356-44365, 2017.

ULLAH, SAJJAD; HAZRA, CHANCHAL; FERREIRA NETO, ELIAS PAIVA; SILVA, TARCIO DE CASTRO; RODRIGUES-FILHO, UBIRAJARA PEREIRA; RIBEIRO, SIDNEY JL. Microwave-assisted synthesis of $NaYF_4$:Yb^{3+}/Tm^{3+} upconversion particles with tailored morphology and phase for the design of UV/NIR-active $NaYF_4$:Yb^{3+}/Tm^{3+}@TiO_2core@shell photocatalysts. **CRYSTENGCOMM**, v. 19, p. 3465-3475, 2017.

POSTER AND ORAL PRESENTATION IN NATIONAL AND INTERNATIONAL EVENTS

Fares, H.; Silva, T. C.; Orives, J. R.; Franco, D. F.; Nalim, M. White light generation from Ag nanoclusters doped oxyfluoride glass for broadband light source. 10th International Conference on Nanophotonics. 2017. (Poster – Best poster award).

Silva, T. C.; Manzani, Danilo; Ribeiro, S. J. L. Visible to near-infrared upconversion emission of highly content Er^{3+}-doped fluoroindate glasses and glass/polymer composites for solar cells applications. Advanced School on Glass and Glass-Ceramics. 2016; (Poster).

Silva, T. C.; Manzani, D.; Ribeiro, S. J. L. XXXVIII Encontro Nacional de Física da Matéria Condensada. Near Infrared upconversion luminescence in RE (RE=Er^{3+}, Yb^{3+}) ions doped fluoroindate glasses and YVO_4 nanoparticles. 2015; (Poster).

SUMMER SCHOOL

Advanced School on Glass and Glass-Ceramics. Universidade de São Paulo (USP); São Carlos – São Paulo/Brasil. 2015.

V Escola Avançada de Óptica e Fotônica. Universidade de São Paulo (USP); São Carlos – São Paulo/Brasil. 2014.

São Paulo School of Advanced Science on Frontiers in Lasers and Their Applications. SPSAS+SWIECA - IPEN – São Paulo – São Paulo/Brasil. 2018.

INTERNATIONAL EXPERIENCE

Internship at “Institute de Chimie de la Matière Condensée de Bordeaux – ICMCB’’ – Bordeaux/France.

Advisors: Thierry Cardinal, Yannick Petit, Lionel Canioni and Véronique Jubera.

Project: Microfabrication of silver structures by direct laser writing (DLW) technique in fluorophosphate glasses. Application in waveguide and second harmonic generation (SHG).

Duration: 04/2017 – 09/2017.

DEDICATION

I would like to express my eternal thoughts and love for those who passed away and made part in my life. Your faces are carved in my memories father “Alcebiades”, uncle “Deilane” and grandmother “Caroline”. There is no one single day that you are not remembered.

ACKNOWLEDGEMENTS

“Scientific life is not composed only by good results and publications”, they sad. That is true. Every single discussion, meeting, coffee in friends company, counts. How could I forget my first advisor? After 10 years in science, I might perceive that I owe part of my evolution and my scientific background to Jesiel Freitas Carvalho. Uncountable days we spent discussing science, life, football and politics. He was patient when I was young, inexperienced, and rigid when it was needed. It was a huge pleasure work with you. Many thanks dear.

Another person important in my life is Sidney, my PhD advisor. A very gentle and educated person carrying a serene smile in his face. It was really meaningful to my career join to the photonic group in 2014. Truly, I would not expect acquire such experience in a short period. I will never forget one of my first days in this group, when Sidney sad “Whether you need money to stay here, I can give you”. After I wondered to myself “who would do such thing? He did!” That is right! I joined to the group without scholarship and he offered to help me. Still, I am very grateful for the work discussion and for the opportunity to work with important researchers like Carlos Graeff, Anderson Gomes, Thierry Cardinal and others.

I would like to thank the “Institute de Chimie de la Matière Condensée de Bordeaux – ICMCB” for the 06 months of internship in 2017. Still, LAPHIA (Cluster of Excellence) group for the mobility grant during my stayed. Up till now, it was the greatest experience in my life abroad. Surely, I perceived that science is a huge universe with such modernity and facilities. I greatly appreciate the supervision of Thierry Cardinal, Yannick Petit, Veronique Jubera and Lionel Canioni. My colleagues Clément Strutynski, Alexander Fargues, Jean-Charles Desmoulin, Sylvain Danto, Wendersen Gebremichael and Alain Aboul Khalil. I appreciate every single minute that I spent in Bordeaux and France. What a beautiful country.

A special thanks to some great friends, Hssen Fares, Guilhermina Ferreira, Jessica Nardeli and Chanchal Hazra. They were my family in my saddest and happiest moments. Uncountable moments we shared togheter. I also need to express my gratitude to my friends Longinus Igbojionu and Shah Ali. My lab-mates in special Douglas Franco, Kishore, Joy, York Serge, Robson Rosa and Danilo Manzani.

My deepest gratitude to my beloved family; my elder brother Tarcísio Castro, my elder sister Taís Castro and my mother Rozely Rosa, for their support and encouragement during the years of my graduation, master, PhD and all my life. I am totally speechless to express my feelings for all of you.

Last but not least, the financial support of the brazilian agencies Capes (Coordenação de Aperfeiçoamento de Pessoal de Nível Superior) and Fapesp (Fundação de Amparo à Ciência e Tecnologia do Estado de São Paulo). Still, my sincere gratefulness to the Chemistry Institut of Araraquara for the infrastructure and all facilities that allowed me to develop my lab work and thesis.

RESUMO

Materiais vítreos se tornaram um dos mais atrativos materiais devido a fácil e rápida preparação. Durante as últimas décadas, várias aplicações têm sido exploradas e a viabilidade para mudança de frequência, conversão ascendente (upconversion) e descendente de energia (downconversion), geração de radiação visível com similaridade das emissões cromáticas azul, verde e vermelho; guia de onda, camadas luminescentes para células solares, geração de segundo harmônico e outros, estão publicadas. Propriedades estruturais como baixa energia de vibração estrutural (fônon), estabilidade química e ampla transparência óptica, tem sido o principal alvo para explorar uma excelente matriz para a dopagem com terras-raras. Por exemplo, íons Er^{3+} é um dos candidatos mais adequados para a propriedade de "upconversion" devido a absorção na região do infravermelho em 0,9 e 1,5 µm e consequente emissão na região do visível e infravermelho. Devido às suas propriedades espectroscópicas, os lantanídeos, geralmente, exibem emissões com linhas estreitas devido à fraca interação com o campo cristalino da matriz. Por outro lado, íons metálicos como a prata (Ag), exibem uma ampla banda de emissão e excitação. A propriedade mais interessante dos íons prata é que a emissão visível pode ser ajustada de acordo com a forma e tamanho das espécies de pratas presentes em uma amostra. Esta propriedade abre um largo espectro de aplicações nas quais a radiação visível pode ser explorada. Neste sentido, um dos principais objetivos dessa tese é mostrar a preparação de materiais vítreos contendo íons lantanídeos como Er^{3+} e Pr^{3+}/Yb^{3+} e /ou íons prata e nanoclusters de prata para aplicação em camadas luminescentes para células solares, geração de luz branca, guia de onda e investigação dos processos de "upconversion" e "downconversion". Para este propósito, materiais vítreos com composição molar $40InF_3$-$20ZnF_2$-20Sr-$20BaF_2$ (vidros fluoroindatos) e $50NaPO_3$-$25ZnF_2$-$15CdF_2$-$10YF_3$ (vidros fluorofosfatos) foram selecionados. Os vidros fluoroindatos foram dopados com íons Er^{3+} com diferentes concentrações e os vidros fluorofosfatos com diferentes concentrações de pratas. Composições com diferentes concentrações de prata e os lantanídeos Pr^{3+}/Yb^{3+} também foram preparadas. As amostras vítreas foram preparadas pelo método de fusão-choque térmico. Os materiais de partida foram homogeneizados em almofariz. A fusão dos compostos para os vidros fluoroindatos foram realizadas em tubo de platina a 850 °C durante 20

minutos e vertidos em um molde metálico pré-aquecido em 260 °C, enquanto que a obtenção dos vidros fluorofosfatos se deu com fusão a 1000 °C durante 30 minutos e vertidos em molde pré-aquecido a 300 °C. A primeira parte desta tese mostra a preparação e avaliação das propriedades estruturais e espectroscópicas dos materiais vítreos. Absorção, excitação e espectros de emissão, o tamanho e morfologia dos nanoclusters de prata (para os vidros fluorofosfatos) bem como as propriedades térmicas foram analisadas. A segunda parte desta tese está relacionada com a aplicação dos vidros fluoroindatos como camadas luminescentes para o aumento da fotocorrente em uma célula solar de silício monocristalino e monofacial. Os vidros obtidos foram cortados e opticamente polidos de modo a obter amostras com as dimensões de 5.4 x 4.3 x 3.2 mm. As amostras foram colocadas na superfície de uma célula solar. Neste ponto, as diferentes concentrações de íons Er^{3+}, que estão associadas à diferentes intensidades de emissão, foram analisadas nas medidas de fotocorrente.

A terceira parte desta tese traz uma breve introdução aos nanoclusters de prata, que será a base para a compreensão dos resultados obtidos dos vidros fluorofosfatos. A maior parte dos resultados foram obtidos em colaboração com o "Institut de Chimie de la Matière Condensée de Bordeaux", exceto os resultados das amostras preparadas para obtenção de radiação branca, capítulo 4. As amostras previamente preparadas com composição molar $45NaPO_3$-$25MgF_2$-$15CdF_2$-$15YF_3$-$5AgNO_3$, foram cortadas e polidas de modo a obter amostras com dimensão 7 x 4 x 2 mm. A estabilização dos nanoclusters de prata se deu através da técnica "Direct Laser Writing (DLW)", utilizando laser de femtosegundo (fs) KGW:Yb, operando com linha espectral em 1030 nm e bombardeando a amostra com diferentes pulsos de energia. A irradiância laser foi controlada um modulador acústico-óptico permitindo a acumulação de N=105-106 com energia variando entre 20 e 150 nJ. As microestruturas de prata gravadas nas amostras foram avaliadas de acordo com suas propriedades de absorção e emissão. Em adição, neste amostra foi avaliada a viabilidade como guia de onda. Por último, na amostra com composição molar (30-x) $NaPO_3$–$30MgF_2$–$30BaF_2$–$10YF_3$–0.5Pr-0.5Yb - xAg (x = 0, 2, 4 and 10) foi analisada a transferência de energia dos nanoclusters de prata e os terras-raras Pr^{3+} e Yb^{3+}. Os resultados apresentados nesta tese representam uma direção promissora para explorar materiais emissores com ampla emissão espectral com potencial uso em

conversão descendente de energia “downconversion”, camadas para aplicações fotovoltaicas, fósforos e guias de ondas.

Palavras-chave: Vidros fluoroindatos; vidros fluorofosfatos, “upconversion”, “downconversion”, transferência de energia, célula solar, nanoclusters de prata, “direct laser writing” e guias de onda.

ABSTRACT

Glassy materials have become one of the most attractive materials owing their easy and fast preparation. During the last decades, several applications have been explored and the feasibility for frequency change, upconversion and downconversion, white light generation, waveguide, luminescent layers for solar cell, second harmonic generation and other, are reported. Structural properties like low energy phonon, chemical stability, broad transparence optical window have been the main target to explore a good host materials for lanthanides dopage. For example, Er^{3+} is one of the most suitable candidate for upconversion since it has 1,5 µm and 0,9 µm absorption. Owing to their spectroscopic properties, lanthanides, generally, show visible emissions with narrow lines due to the poor interaction with the crystalline field of the host material. On the other hand, metal ions such as silver; generally, shows a broadband emission and absorption. The most interesting spectroscopic properties of silver is that the visible emission may be tunable according to the size and shape of the silver species in the host materials. This property opens a large spectrum of application in which the visible light can be explored. In this sense, the main goal of this thesis is to show the preparation of glassy materials containing lanthanides such as Er^{3+}, Pr^{3+}/Yb^{3+} and/or silver ions and nanoclusters for luminescent layers for solar cell and photonic applications. The glassy materials selected for such purposes were fluoroindate glasses and fluorophosphate glasses. The samples were prepared by the conventional melting-quenching method. The raw materials with high purity were weighted and mixed according to the following molar composition: $40InF_3$-$20ZnF_2$-20Sr-$20BaF_2$ (fluoroindate glass) and $50NaPO_3$-$25ZnF_2$-$15CdF_2$-$10YF_3$ (fluorophosphate glass). Besides, other compositions of fluorophosphate glasses were also synthesized. Fluoroindate glasses were doped with different Er^{3+} amount and the fluorophosphate glasses with different silver amounts. The raw materials of the fluoroindate glasses were melted in a platinum tube at 850 °C during 20 minutes and poured out in a mold pre-heated at 260 °C. On the other hand, the raw materials of the fluorophosphate glasses were melted in a platinum crucible at 1000 °C during 30 min and poured out in a mol pre-heated at 300 °C. The first part of this thesis was the preparation and the evaluation of the structural and spectroscopic properties of these glasses. Absorption, excitation and emission spectra, size and morphology of the silver nanoclusters (for

the fluorophosphate glasses) as well as thermal properties were analyzed. The second part of this thesis is related to the application of the fluoroindate samples as luminescent layers for enhance photocurrent in a monocrystalline and monofacial silicon solar cell. The glasses obtained were cut and polished in order to obtain samples with dimensions 5.4 x 4.3 x 3.2 mm. The functional glass pieces were placed on the surface of the solar cell. At this point, the different Er^{3+} amount, which is associated with different upconversion intensity responses were evaluated in the photocurrent measures.

The third part of this thesis brings a brief introduction to the silver nanoclusters that will be the bases to understand the results obtained from the fluorophosphate glasses. Majority of these results was obtained in collaboration with "Institut de Chimie de la Matière Condensée de Bordeaux", except the results of the samples for white light generation, shown in the chapter 4. The samples previously prepared with molar composition $45NaPO_3$-$25MgF_2$-$15CdF_2$-$15YF_3$-$5AgNO_3$, were cut and polished in order to obtain samples with dimension 7 x 4 x 2 mm. The stabilization of silver nanoclusters was carried out by direct laser writing (DLW technique), using a femtosecond laser (KGW:Yb) operating at 1030 nm and delivering different energy pulses. The laser irradiance were controlled with an acousto-optic modulator enabling the accumulation of N=105-106 pulses with energy pulses going from 20 nJ up to 150 nJ. The microstructures of silver nanoclusters were evaluated according their absorption and emission properties. Still, for this sample we also analyzed the feasibility as waveguiding material. For last but no least, the sample with molar composition (30-x) $NaPO_3$–$30MgF_2$–$30BaF_2$–$10YF_3$–0.5Pr-0.5Yb - xAg (x = 0, 2, 4 and 10) was prepared in order to evaluate the energy transfer among the silver species and the rare earths Pr^{3+} and Yb^{3+}. The results presented in this thesis represent a promising direction to explore broadband emitter's with potential use in down-conversion, layers for photovoltaic application, phosphors and waveguide. .

Keywords: Fluorindate glasses, fluorophosphate glasses, upconversion, downconversion, energy transfer, solar cell, silver nanoclusters, direct laser writing and waveguide.

“Next time someone complains that you have made a mystake, tell him that may be a good thing. Because without imperfection, neither you nor I would exist.”

(Stephen Hawking, 2010)

LIST OF FIGURES

LIST OF TABLES

LIST OF ABBREVIATIONS

Ag – Silver

Ag NC's – Silver Nanoclusters

Ag NP's – Silver Nanoparticles

a-Si - Amorphous silicon

CB – Conduction Band

CET – Cooperative Energy Transfer

CIE - Commission Internationale d'Eclairage

CR – Cross Relaxation

CTB – Charge Transfer Band

DC – Dow nconversion

DLW – Direct Laser Writing

Eg – Bandgap

EMU – Energy Migration Upconversion

ESA – Excited State Absorption

ET – Energy Transfer

ETE – Energy Transfer Efficiency

ETU – Energy Transfer Upconversion

FWHM – Full Width of Half-Maximum

GSA – Ground State Absorption

HRTEM – High Resolution Transmission Electron Microscopy

kV – Kilovolt

LED – Light Emitting Diode

LLSC – Luminescent Layer for Solar Cell

Ln^{3+} - Lanthanides

mc-Si - Multicrystalline silicon

PA – Photon Avalanche

PV – Photovoltaic

SAED – Selected Area Electron Diffraction

SC – Solar Cell

Si SC – Silicon Solar Cell

Single-crystalline silicon – sc-Si

SPR – Surface Plasmon Ressonance

TEM – Transmission Electron Microscopy

Tg – Transition Temperature

UC – Upconversion

UV – Ultraviolet

Vis – Visible

WG – Waveguide

TABLE OF CONTENTS

Luminescent layers for solar cell application

During the past 30 years there has been a remarkable growth in the use of luminescent materials for solar cell application. A huge variety of amorphous and crystalline materials has been employed in order to increase the photocurrent of different photovoltaic systems. In this sense, lanthanides ions have been employed as good candidates for luminescent layers, which may be used in the rear and the top face of certain solar cells. In this chapter, we present an overview of the solar cells landscape, the drawbacks associated with the solar spectrum mismatch and the pathways to overcome such issues. A greater emphasis is given to the solar cell from the first generation that are silicon-based solar cells. Along this chapter, it may be note that this kind of cell is taken as example to explain an increment of efficiency using luminescent layers. However, it is far beyond of this chapter to deal with efficiency using an AM 1.5G conditions as well as the measure of short-circuit current, fill factor and other parameters related. For this purpose, whenever necessary, the reader is direct to some references throughout the chapter. Besides, rare-earth spectroscopy is also mentioned as well as one of the most explored properties, the "upconversion" phenomenon.

1 Introduction

The large-scale use of fossil fuels has brought serious issues of global warming and environmental pollution due to the nonrenewable energy consumption [KANG et al, 2010; LUNT; BULOVIC, 2011]. Since the introduction of first commercial solar cell (SC) in the 70ths years, research efforts in SC scaled up the knowledge to sustainable sources. Presently, solar energy is an emerging and alternate source of energy that can direct the usage to the clean and abundant form of energy [AHMED; HABIB; JAVAID, 2015]. Moreover, solar energy is one of the few renewable, low-carbon resource with maturity to meet ever-growing global demand for electricity [JEAN et al., 2015].

Daily, the sun delivers about 174 000 TW of energy to the upper level of the atmosphere, meaning 10 000 times more energy than our global energy consumption [RUHLE; SHALOM; ZABAN, 2011]. This energy corresponds to an average energy power 1366 $TW.m^{-2}$. Taking into account atmosphere absorption and scattering, this value is reduced to 1000 $W.m^{-2}$. Moreover, with further losses due to seasonal

variation, oblique incident radiation, weather attenuation and cloud cover, leads to a global daily average of 183 $W.m^{-2}$ [JACOBSON; DELUCCHI, 2011].

The most direct way to convert solar radiation into electricity is the use of photovoltaic (PV) cells, also commonly named as solar cells (SC). In such device, a semiconductor composed by a positive and negative (p-n) junction develops photovoltage. The detailed process to generate current is ascribed as following: when solar radiation (photons) is absorbed, electrons raise to a higher energy state, and then they flow to an external circuit, since electron-hole recombination pair is avoided. Electron and holes move to opposite electrodes and their recombination generate electric current. Such photovoltaic effect happens when few conditions are observed: (i) photons absorbed by the solar cell must to have energy equal or higher than the bandgap (E_g) of the cell; (ii) the absorption of photons must to guarantee the formation of electron-hole pair, also called charge carriers; (iii) spatial separation of the charge carriers is observed by a p-n junction, so that any recombination is prevented; (iv) after electron flowing in the external circuit, electron-hole must to be regenerated again on the positive layer. For the sake of brevity, only main factors to generate photocurrent are mentioned above, however, the electric current density is affected by factors like shading, cell temperature, cable thickness, solar radiation intensity, climate conditions, cell lifetime and other [CHOPRA; PAULSON; DUTTA, 2004; GOETZBERGER; HEBLING; SCHOCK, 2002]. Moreover, Figure 1.1 represents the simplest configuration in which the SC is based in a double-layer (p-n junction) diode. Along this chapter, we are going to show complexes system, like those shown in Figure 1.2, in which several layer may be present in a PV device.

Figure 1.1. Schematic of a single-junction solar cell.

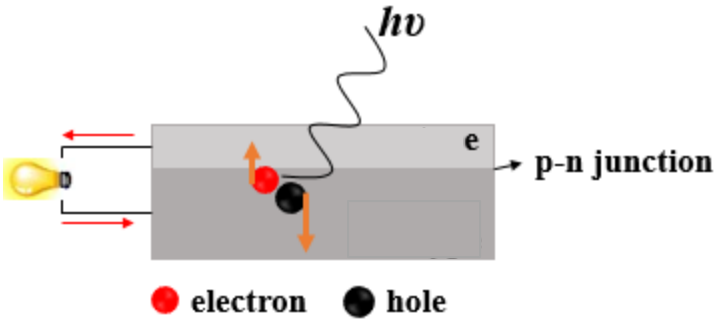

Along the last 5 decades, solar cell technology has grown dramatically owing the evolution of new materials that found their specific niche through different SC generation. In 2015, Jean et al. has presented a review paper regarding solar cell technology where the classification follows a trend in which the primary light-absorbing material was taken into account. According to them, two categories are defined: wafer-based cells and thin-film cells, respectively. Still, the generations are also referred as first, second and third generation, where the first one refers to the wafer-based SC, the second one refers to thin-film SC and the third one refers to the commercial thin-film SC. Here, we adopted the same definition described by Jean et al. [JEAN et al, 2015].

Figure 1.2 a-c shows the SC technology according wafer-based and thin-film classification. Wafer-based SC, or also called first generation, comprises the most mature of all photovoltaic technology and commercially speaking, that is silicon SC (Figure 1.2a). Silicon SC are classified as single-crystalline (sc-Si), multicrystalline (mc-Si) and amorphous (a-Si). Record cell efficiency for sc-Si, mc-Si and a-Si stand at 25.6%, 20.8% and 10.2% [GREEN, 2015], respectively. Nowadays, the global production counts with 90% of c-Si. In a general view, Si SC is composed by a positive (p-Si) and negative layer (n-Si) in which the thickness of the negative is smaller than the positive one. Back and frontal contacts are constituted of aluminum (Al) layer and thin strips of deposited silver (Ag). Other two SC compose the first generation, they are GaAs (Gallium arsenide) and III-IV MJ (Multijunction), Figure 1.2a. The major feature of III-IV MJ is the multiphoton absorption. In other words, this SC is able to absorb in different bandgaps across the solar spectrum. Two or more single-junction

layer composes this cell, in which each layer is stacked by decreasing the energy gap of the semiconductor. The main advantage of this configuration is the reduction of thermalization losses and the efficiency for two, three and four junctions can reaches 46%, 44.4% and 34.1%, respectively. However, high cost materials and complex manufacturing limit a high-scale production.

Figure 1.2b shows the second SC generation, which is composed by commercial thin-film like a:Si-H (Hydrogenated amorphous silicon), CdTe (Cadmium telluride) and CIGS (Copper indium gallium diselenide). Cell efficiency for these SC are 12.2% for a:Si-H, 21% for CdTe and 21.7% for CIGS. A higher absorption efficiency is the key advantage compared to Si SC, and this allows the use of thin films of few microns of thickness. Besides, low material application may reduce the final cost; also, transport and installation may become easy task for this technology. However, limiting factor like high toxicity of cadmium, telluride; low abundance of indium and light-induced degradation for a:Si-H can hinder the large-scale application of these cells [JEAN et al, 2015].

Third generation extends the concept of thin film for nanostructured materials such as organic, perovskite, quantum dots, dye-sensitized solar cell (DSSC) and copper zinc tin sulfide (Cu_2ZnSnS_4, CZTS), Figure 1.2c. Key advantages for this generation is the ability to form flexible, light and thin SC, simple process manufacturing, low-temperature processing compared to those SC from the first generation and second [HAMAN et al, 2008; GREEN et al, 2002]. Solar efficiency for these SC are 20,1% (Perovskite), 11,1% (Organic), 12,3% (DSSC), 9,2% (Quantum dots) and 12,6% (CZTS). Despite the high plenty of organic elements that is advantageous for large-scale deployment, these SC, naturally face constraints issues like low durability and toxicity in Perovskite cells, low lifetime for all SC compared to the Si SC, in which each module has medium lifetime of 25 years [QIAO et al, 2018]. Still, unlike Si, cells from the second and third generation suffer with scarce elements and photodegradation under long time ultraviolet dose.

Figure 1.2. Solar cell generation according to wafer-based and thin-film classification. (a) First generation: wafer-based; (b) second generation: commercial thin film; and (c) second generation: thin-film.

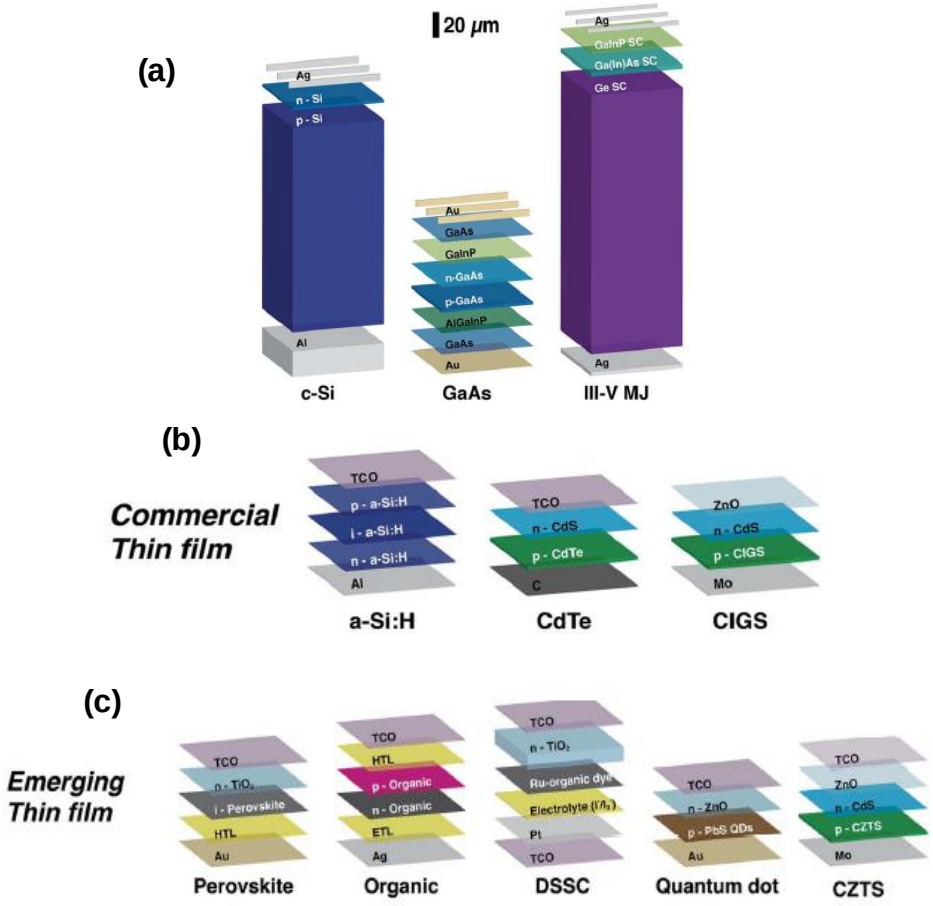

SC technology landscape still drives attention and efforts to cells from the first generation, especially, Si SC. Silicon counts with high abundance in earth crust, non-toxicity and higher cell efficiency. However, one major drawback hinder the enhancement of the efficiency that is solar spectrum mismatch. The maximum theoretic efficiency demonstrated for a single junction SC is 32%, this limit was first theoretically established by Shockley-Queisser [SHOCKLEY; QUEISSER, 1960]. Indeed, SC efficiency is limited also by the fact that sunlight reaches the surface cell in a non-concentrated and diffuse form, so that external devices (mirrors) are required to focus the radiation direct to the cell [CORREIA et al., 2014].

Solar spectrum mismatch brings two consequences to SC with a specific bandgap (E_g), that is the thermalization of charge carriers and sub-bandgap loss, or also called loss by transmitted photons. Thermalization process is generated by absorption of high-energy photons, photons with energy higher than SC E_g. Meanwhile, sub-bandgap losses is generated by transmission of lower energy-photons, photons with lower energy than SC E_g. Both kind of photons, higher and lower energy than SC E_g, cannot be efficiently converted in electric energy. Taking as example Si SC with a bandgap of 1.1 eV (1100 nm), a broad part of the solar spectrum will be lost by thermalization and transmission. Solar spectrum on the surface earth widely ranges from 300 to 2500 nm with maximum intensity around at 500 to 600 nm [RODRÍGUEZ-RODRÍGUEZ, 2016] as it is shown in Figure 1.3. Grey color depicts the solar radiation incident in the earth's surface and the red region depicts the Si sensibility on the solar spectrum. Part of the incident energy (35%) is lost by thermalization and 20% by transmission (sub-bandgap photons) [ASIM et al., 2012].

Losses process by thermalized photons and transmitted photons can be represented by the scheme in the Figure 1.4. Thermalization process are generated when charges arise straightforward to the edges of the conduction band (CB) and valence band (VB), process (a). Such excess of energy is readily dissipated as heat and its loss is substantial for SC with small bandgap. Contrarily, the SC cannot absorb transmitted photons, since its energy is not suitable to generate an electron-hole pair. The process (b) represents loss process by transmitted photons [RICHARDS, 2006].

Figure 1.3. Solar spectrum at earth's surface. The red region emphasizes the portion of the terrestrial sunlight that is absorbed by a silicon SC with bandgap of 1.12 eV, and spectral regions that are lost by thermalization and below bandgap or transmitted photons [ASIM et al, 2012].

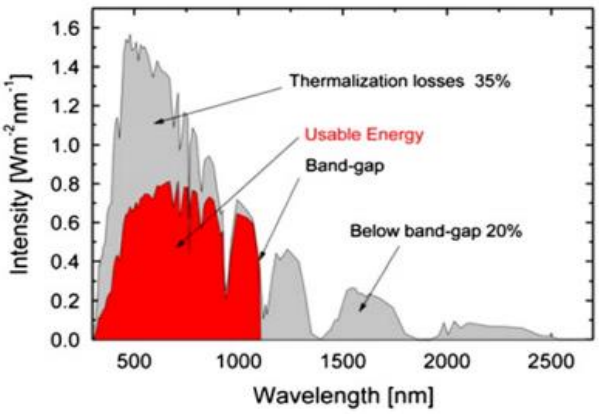

Spectral mismatch in solar cell motivated many efforts to develop new materials with specific features to overcome such limitation [SARK et al, 2014]. The optimism in SC science inflates with the discover of the enhancement of efficiency conversion by modifying the input spectrum. Such conversion would be possible using lanthanide-based materials in which exhibit upconversion and downconversion phenomenon [CORREIA et al, 2014; ENDE; AARTS; MEIJERINK, 2009]. The next topic, we present a brief physics and chemistry introduction concerning lanthanides elements as well as their application in solar cell. For the sake of brevity, only the most employed lanthanide elements will be treat. Still, we are going to restrict the application of lanthanides elements in amorphous materials as well as their use as luminescent layers.

Figure 1.4. Losses in a single-junction SC. Process (a), thermalization photons and (b), transmitted photons. Adapted from reference [RICHARDS, 2006].

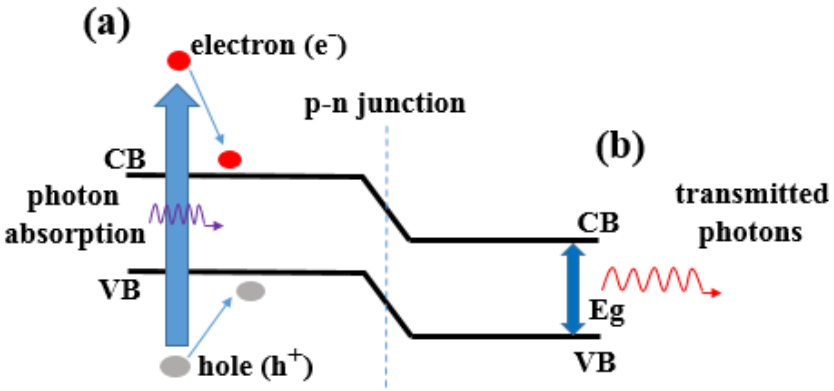

1.2 Lanthanides

Lanthanides ions (Ln^{3+}) are commonly formed by ionization of an outer electron of atoms located at the bottom of the periodic table after lanthanum: from Cerium (atomic number 58) to Ytterbium (atomic number 70), which possess the electronic configuration $5s^25p^65d^14f^16s^2$ and $5s^25p^64f^{14}6s^2$, respectively [SOLÉ; BAUSÁ; JAQUE, 2005]. Lanthanides ions have general configuration $[Xe]4f^{n-1}5d6s^2$, where [Xe] stands for the Xenon electronic structure and *n* is the number of electrons in the unfilled 4*f* shell, that varies from 1 (Ce^{3+}) to 13 (Yb^{3+}). Although some ions may assume divalent (Sm^{2+}, Eu^{2+}, Yb^{2+}) and tetravalent state of oxidation (Ce^{4+}, Tb^{4+}, Pr^{4+}), the trivalent state is the most stable. To reach such ionization, the Ln^{3+} may lose a 5*d*, 6*s*

and one of the 4*f* electrons, leaving a partially filled 4*f* orbital that is shielded by the 5*s* and 5*p* orbitals [DWIVEDI; ZILIO, 2013]. Table 1 summarizes the lanthanide atoms in a trivalent configuration, the number of electrons valence on the 4*f* orbital of each atom and the electronic configuration as well.

Table 1.1: Number (*n*) of electrons distributed in the unfilled 4*f* orbital of Ln^{3+} ions and the electronic configuration. Adapted from the reference [SOLÉ; BAUSA; JAQUE, 2005].

Atomic Number	**(Ln^{3+}) ion**	***n***	**Electronic configuration (Ln^{3+})**
58	Ce^{3+}	1	$4f^1 5s^2 5p^6$
59	Pr^{3+}	2	$4f^2 5s^2 5p^6$
60	Nd^{3+}	3	$4f^3 5s^2 5p^6$
61	Pm^{3+}	4	$4f^4 5s^2 5p^6$
62	Sm^{3+}	5	$4f^5 5s^2 5p^6$
63	Eu^{3+}	6	$4f^6 5s^2 5p^6$
64	Gd^{3+}	7	$4f^7 5s^2 5p^6$
65	Tb^{3+}	8	$4f^8 5s^2 5p^6$
66	Dy^{3+}	9	$4f^9 5s^2 5p^6$
67	Ho^{3+}	10	$4f^{10} 5s^2 5p^6$
68	Er^{3+}	11	$4f^{11} 5s^2 5p^6$
69	Tm^{3+}	12	$4f^{12} 5s^2 5p^6$
70	Yb^{3+}	13	$4f^{13} 5s^2 5p^6$

Since the orbitals $5s^2$ and $5p^6$ are totally filled electronically, optical and magnetic properties are ruled by the unfilled 4f shell and in some ions like Ce^{4+} and Eu^{2+}, by the 5d vacant orbital [REID, 2016]. However, yttrium (Y) also has +3 oxidation state and does not show optical transitions. In addition, Lanthanum (La^{3+}) and Lutetium ions (Lu^{3+}) have a completely empty and a completely filled 4f shell, therefore they are not optically active. Moreover, the *4f-4f* direct interaction between neighboring rare-earth

ions may be considered as negligible and the behavior of the 4f electrons seems to be different from that s, p and d electrons [WYBOURNE, 2004].

The shielded effect of the 4f orbital results in a poor interaction with the closest neighbor in a crystalline medium, by consequence, these inner electrons do not participate directly in chemical bonds. Such case, leads to the well-known situation "*weak crystalline field"*, which an ion is slightly perturbed by the crystalline field. The effect of the crystal field is to produce a slight shift in the energy levels and to cause additional level splitting within the *f* shell.

The electrons confined within the 4f orbital experiment a rearrange that is parity-forbidden. However, owing to a forced dipole electric transitions, most of the radiative transition become partially allowed by mixing the 4f orbitals with other orbitals that have different parity. In this sense, a promotion of a 4f electron into the 5d orbital are allowed by parity rule. In addition, a charge transfer band (CTB) can also implies an electronic transition in a trivalent lanthanide. This transition is allowed by the Laporte's selection rule [BUNZLI, 2007].

Taking into account the low perturbation of the 4f electrons by a electric field, the *f-f* transitions become quite narrow and sharp compared to metal ion environment that directly affects the electrons involved on the optical properties. Consequently, a RE^{3+} ion may have similar optical spectra among several different crystalline or amorphous medium [JORGENSEN; REISFELD, 2005; TANABE, 2015].

1.3 Energy levels of the RE^{3+}

When a RE^{3+} ion is dispersed in a crystalline host, it will experiment an electric field that will slightly perturb the $^{2S+1}L_J$ states, where S and L are the total spin and total orbital quantum number, *J* is the total angular quantum number, which can assume the values J = (L+S); (L+S) – 1; (L+S) – 2;…; (L-S) [SOLÉ; BAUSÁ; JAQUE, 2005]. In spectroscopic notation, *L* may assume different symbols that are derived from the spectroscopic lines corresponding to s, *p*, *d*, *f* (sharp, principal, diffuse and fundamental) orbitals. For example, we may predict the ground state to the Ce^{3+} ion, which has an electronic configuration $4f^1 5s^2 5p^6$. According to the Pauli Exclusion Principle, this only one electron 4*f* may be distributed in the following diagram box:

Figure 1.5. Electronic distribution of the Ce^{3+} ion in a box diagram.

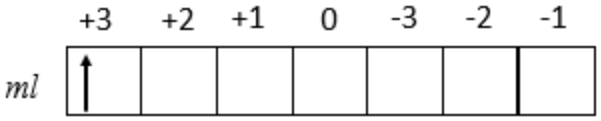

Since ml = +3 and $L = \Sigma ml$, the orbital quantum number (L) will be 3. Each L is associated to a symbol that is characteristic of the spectroscopic lines corresponding to the orbitals sharp, principal, diffuse and fundamental (s, p, d, f).

$$\begin{matrix} L = 0\ 1\ 2\ 3\ 4\ 5 \\ S\ P\ D\ F\ G\ H \end{matrix} \quad (1)$$

Assuming that L = 3, the electron from the Ce^{3+} will be in an orbital associated to a quantum number F. Another quantic number to determine is spin total (ms) that is associated to the electronic orientation and can have positive and negative values. Assuming a positive configuration to the spin electronic (+1/2), the ms will be equal to +1/2, and considering that $S = \Sigma ms$, the total spin is S = +1/2 and 2S+1 is equal to 2. As J = (L+S); (L+S) – 1; (L+S) – 2;…; (L-S) and S is +1/2, the state with the lowest J value (L-S) is 5/2. Therefore, spectroscopic term for the ground state of the Ce^{3+} ions is $^2F_{5/2}$.

The barycenter of energy of each $^{2S+1}L_J$ states may change according to the electric field surround the Ln^{3+}, since the electric field depend on the site symmetry and the nature of the ions in the crystal [YUHUA, 2015]. However, since the Re^{3+} ions assume a free-ion behavior, the position of the multiplets are almost independent of the crystal. Therefore, the gross feature of the energy level diagram remain unchanged [SOLÉ; BAUSÁ; JAQUE, 2005]. The maximum number of sublevels components for each $^{2S+1}L_J$ level is given by 2J+1 when J is an integer and 2J+1/2, when J is half-integer.

The absorption spectra of the Re^{3+} ions in lanthanum chloride crystal were target of extensive research by Dieke's group [BUNZLI, 2007]. The entire $^{2S+1}L_J$ levels of energy of all the trivalent ions are shown in the Figure 1.6. The distribution varies from Ce^{3+} ($4f^1$) to Yb^{3+} ($4f^{13}$). The short horizontal lines indicates the energies of the $^{2S+1}L_J$ multiplets and the width of the lines representing the crystal-field splittings of the multiplets. The largest split among the states by the order of 10^4 cm^{-1} are caused by

Coulomb interaction. The spin-orbit (S-L) interaction splits the terms in multiples separated by the order of 10^3 cm^{-1}. For the last, the crystal-field interaction split the multiplets by order of 10^2 cm^{-1} [WHEG et al, 2000].

Figure 1.6. Energy level for trivalent rare-earth ions (RE^{3+}) in LaF_3 crystal [ELISEEVA; BUNZLI, 2010].

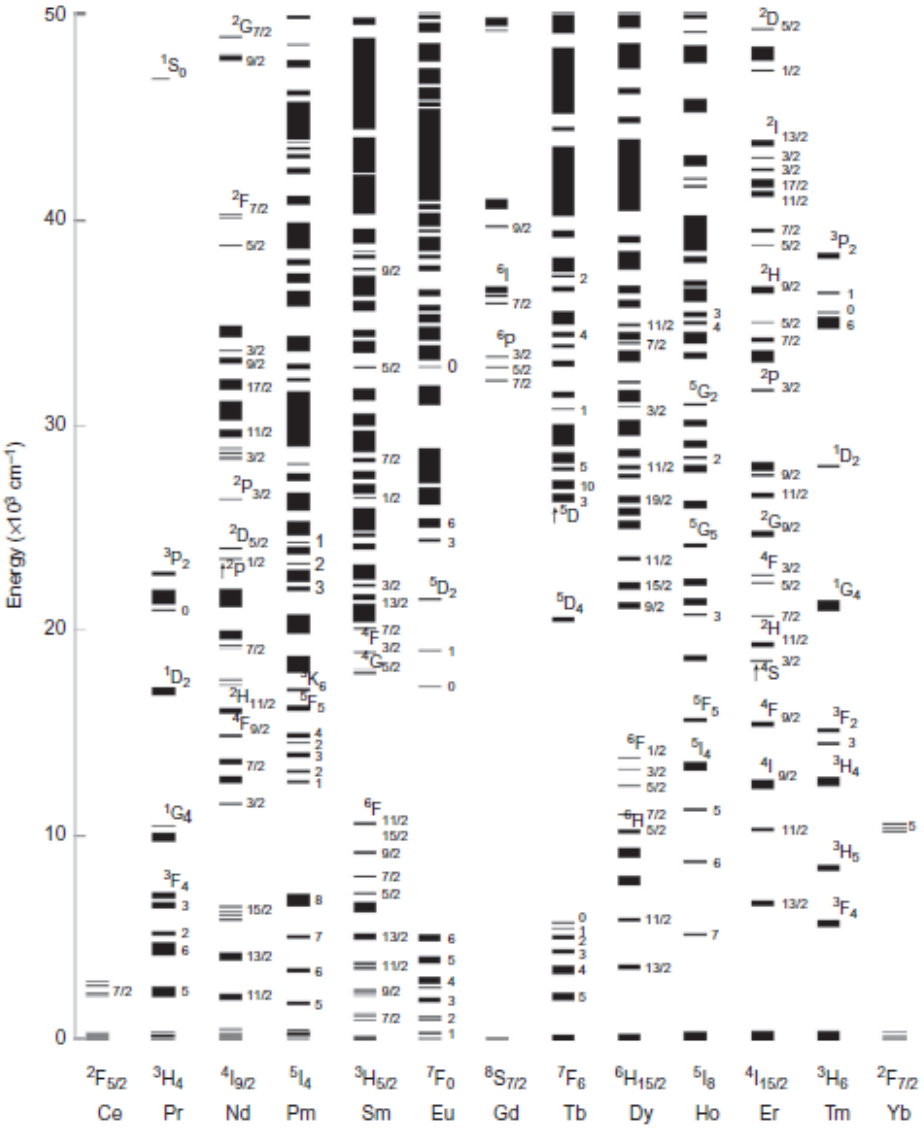

1.4 Upconversion

One of the most explored spectroscopic properties of the RE^{3+} is the upconversion (UC). The origin of the first research in UC can be date in 1959 by Bloembergen, who proposed lanthanide-doped materials as infrared quantum counters [BLOEMBERGEN, 1959]. Nowadays, the interest in this phenomenon is far beyond

and covers a wide research field. A huge variety of potential applications is explored, for example, bio-imaging [LIU; HOU; GAO, 2014], white light modulation [KARATAIRI; HOPPE, 2016; ELISEEVA; BUNZLI, 2011], thermal sensors [LALLA et al, 2015], photocatalysis [ULLAH et al, 2017], spectral converters for sola cell [GOLDSCHMIDT; FISCHER, 2015; SHPAISMAN, 2008], solid-state lasers and others [LIAN et al., 2013; -19; DONG, 2017; VASILIEV, 2016].

The term UC refers to a non-linear process in which the continuous absorption of two or more low-energy photons leads to the emission of high-energy photons (anti-Stokes emission) [REID, 2016]. Figure 1.7 summarizes the simplified mechanisms of UC emissions, which may be described as following: the first step corresponds in an excitation through a near-infrared source, indicated by the orange arrow in the Figure 1.7 (a)-(e). In this step, one electron that is in its ground state (E_0) is excited and occupies the first metastable state (E_1). This first step is fundamental and common to all the mechanisms; excited state absorption (ESA), energy transfer upconversion (ETU), photon avalanche (PA), cooperative energy transfer (CET) and energy migration upconversion (EMU). The second step differs from each mechanism. For example, the first mechanism (Figure 1.7a), the UC occurs in a single ion. After absorption of one photon, the same excited electron (now in E_1 state) absorbs another photon of the same energy and goes to a further higher excited state (named as E_2). From this state, radiative transition is observed with emission of a higher-energy radiation.

In an ETU mechanism (Figure 1.7b), two ions are involved and they are commonly named as sensitizer and activator, in which the sensitizer, generally, has a higher cross section than the activator. Since the first intermediated state from the sensitizer and activator are spaced in a close distance (resonant), the sensitizer transfer energy to adjacent ion that is excited to the E_2 state. Commonly, the mechanism that happens between two ions is called "*upconversion cooperative system*" and can be observed between two similar ions or different ions [SUN, 2015]. However, for different ions the primordial condition is that the metastable state of the two ions must to be energetically close.

When the energy gap between an intermediated state and the ground state is non-resonant with the pump power, the PA can produce population in an excited state whose energy exceeds that the pump photon [JOUBERT et at, 1999; STRUMPEL et

al, 2007], as it is shown in the Figure 1.7c. This electron will be excited to a higher state energy (E_2) by an ESA. Then, a cross relaxation (CR) excites an adjacent ion and the level of the same ion. It is peculiar to mention that a UC photon can be generated without a GSA step. In this case, the consumption of superexcited ions must to be less than the ground state ions [SUN, 2015].

Another mechanism that takes place in a cooperative sense is the CET, shown in the Figure 1.7d. In this process, two sensitizer ions are needed to sensitize the activator. This is due to an absence of a long-lived metastable state of the sensitizer. The last mechanism is the EMU, shown in the Figure 1.7e. In 2011, Liu and coworkers introduced this new UC mechanism based in core-shell structured nanoparticles. In the EMU, the energy transfer from the core to the shell follows a cascade-type sensitization in which the sensitizer is located on the core and the activator on the last shell [WANG, 2011].

Figure 1.7. Simplified energy levels for different two photons mechanisms in UC process. The excitation of the sensitizers ions are represented by orange arrows, non-radiative transition are represented by black dotted arrows and the purple arrows represent visible emission from the excited state E_2 to the ground state E_0, respectively.

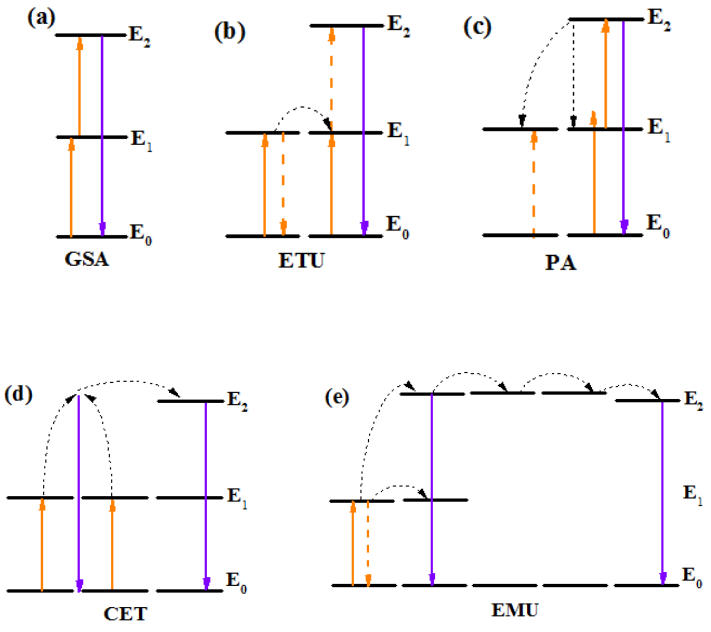

Despite the benefits resulting from the UC emissions (see applications in the beginning of this section), the main limitation of the RE^{3+} is the narrow and weak absorption associated with the nature of the *4f-4f* transitions [BUNZLI; PIGUET, 205], which is shielded by the orbitals 6s and 6p. For comparison, the Yb^{3+} that is the most efficient sensitizer used for generation of UC emission, has approximately a cross section of 10^{-20} cm^2, that is 1000 to 10000 lower than a dye molecule (10^{-17} – 10^{-16} cm^2). Still, the narrow spectral absorption, over 10 times narrower than an organic dye, compromises their utility for several applications. For example, the excitation using natural sources, like the sun, is not feasible to generate UC emission. Indeed, this phenomenon happens by using commercial sources, like diode laser operating at 808, 980 and 1500 nm [RODRÍGUEZ-RODRÍGUEZ, 2013]. Last but not the least, the total efficiency of an UC system can reach a maximum 50% since two photons is necessary to provide one photon.

1.5 Upconversion for photovoltaic application

Bringing back the concept of solar mismatch in solar cell, here considering the transmitted photons, first mentioned on the introduction of this chapter, we are able to scale-up one of the most interesting application of the upconversion phenomenon. Trupke et al. [TRUPKE; GREEN, WURFEL, 2002] performed the first theoretical approach investigating UC in photovoltaic devices. The authors report a theoretical system in which an upconverter layer is located in the rear level of a bifacial solar cell and the harvesting of sub-band-gap photons allowed them to find 63,2% of quantum efficiency for concentrated sunlight and 47,6% for nonconcentrated sunlight. Figure 1.8 summarizes the system used by Trupke et al.

Figure 1.8. Scheme of an ideal system for UC in a bifacial sola cell proposed by Trupke et al. Adapted from the reference [TRUPKE; GREEN, WURFEL, 2002].

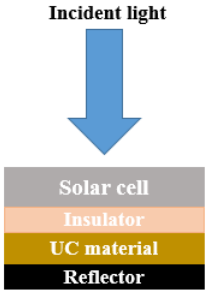

The packed system is composed by a bifacial sola cell, an insulator to isolate electronically the solar cell and the UC layer. Beneath the UC material, a reflector is located to reflect back the light emitted by the UC layer. Trupke et al. assumed that a photon selectivity would be applied to generate extra electron-hole pairs on the solar cell. In other words, the UC material would absorb the radiation transmitted by the first layer, here considered as solar cell. Then, the transmitted radiation absorbed by the UC material is delivered with a higher energy photon. The rear reflector located below the UC layer, reflects the light back to the solar cell. In this way, all the radiation converted by the UC layer is used to generate an electron-hole pair on the photovoltaic device.

Viorel Badescu [BADESCU, 2008], in 2008, presented an extended stud of the seminal work of Trupke et al. Badescu compared two different approach: (i) a system composed by a solar cell and Upconversion layer (SC-UC) and (ii) upconversion layer and solar cell (UC-SC). In another words, the system (ii) presents the upconversion layer on the top level of the solar cell. Indeed, in this new approach, is totally predictable that part of the radiation emitted by the UC layer, would be lost on the top surface (emission in all spatial directions). Moreover, part of the incident radiation would be lost by scattering on the UC layer. Therefore, no benefit can be expected when a UC layer is placed at the front of the solar cell.

Figure 1.9. Experimental scheme of an UC material and a solar cell proposed by Badescu. Adapted from the reference [BADESCU, 2008].

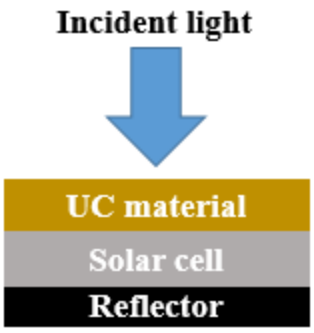

Few years earlier, in the 90th years, experimental insight has shown promising results by using the rare earth Er^{3+} and Yb^{3+} as upconverter materials in GaAs solar cell. In 1996, Gibart et al. [GILBART, 1996] developed a device based in a vitroceramic co-doped with Yb^{3+}/Er^{3+} to use part of the infrared radiation otherwise lost by transmission in a GaAs solar cell. Figure 1.10a shows the setup used and 1.10b shows the energy levels of the Yb^{3+}/Er^{3+} pair according to the mechanism proposed by the authors. An infrared laser (980 nm) irradiates the front face of a GaAs solar cell. The radiation pumping is called "*bellow bandgap IR irradiation*" because the radiation energy is lower than the bandgap of the solar cell, so that the incident radiation is transmitted to the upconverter material. By two-photon UC mechanism, the vitroceramic emits green and read radiations, according to the mechanism from the Figure 1.10b in which the Yb^{3+} ion absorbs two photons and after energy transfer to the closest Er^{3+}, then useful radiation is emitted to generates electron-hole pairs in a GaAs solar cell. In this experiment, a Ti-Sapphire IR laser at 1.39 eV lighted the GaAs cell, which has bandgap of 1.42 eV. For an input excitation of 1 W, the authors found an efficiency of 2.5% illuminating a substrate of 0.039 cm^2 of sensitive area

Figure 1.10. (a) Experimental setup of a GaAs solar cell coupled with Yb^{3+}/Er^{3+} co-doped vitroceramic, and (b) energy levels showing red and green emissions after energy transfer from Yb^{3+} to Er^{3+}. Figure (a) was adapted from the reference [GILBART, 1996].

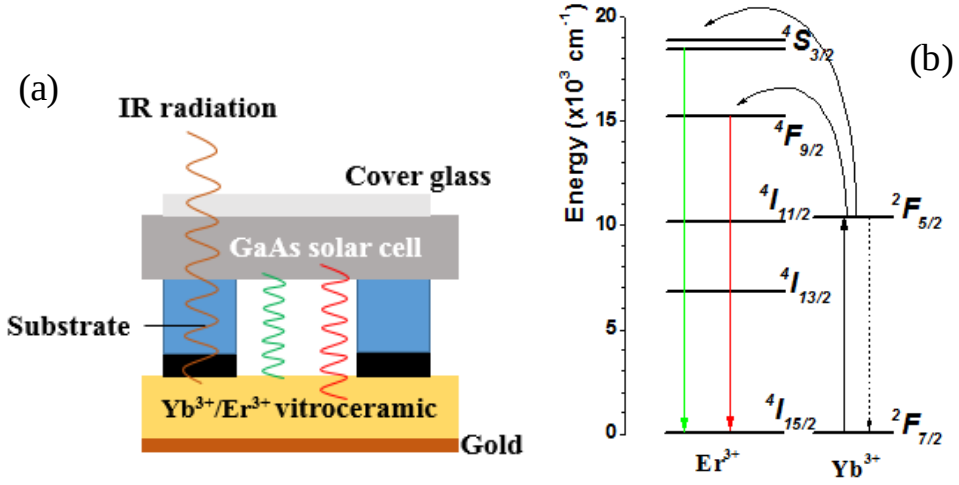

Regarding to the most commercial deployed solar cell, silicon was first applied in a proof-of-principle in 2003, when Shalav et al. [SHALAV, 2007] reported a bifacial solar cell with the upconverter $NaYF_4:Er^{3+}$ in the rear side of the device. Indeed, the rare earth Er^{3+} is one of the most useful ion for upconversion applications. The first excited state is the $^4I_{13/2}$ and the energetic different between this state and the ground state ($^4I_{15/2}$) is 0,827 eV that is equivalent to 1500 nm [CHEN, 2015]. Still, the states $^4I_{9/2}$ and $^4S_{3/2}$ are multiples of the $^4I_{15/2} \rightarrow {}^4I_{13/2}$ transition, so that an excitation at 1500 nm is ideally suited to populates the excited states and then releases visible and near-infrared photons due to its upconversion. Figure 1.11 shows UC between two ions Er^{3+} in which one is the sensitizer and the second one is the activator. Upon excitation around 1500 nm, the excited levels of the activator can be populated after subsequent energy transfer (ET) from the sensitizer, and then, radiative transitions can be observed through the emission of light at 980, 810, 660, 550 and 410 nm.

Figure 1.11. Energy levels of two Er^{3+} ions showing UC process upon excitation at 1500 nm. Three subsequent ET from the sensitizer to the activator guarantee the population of the excited states in which UC emission is observed.

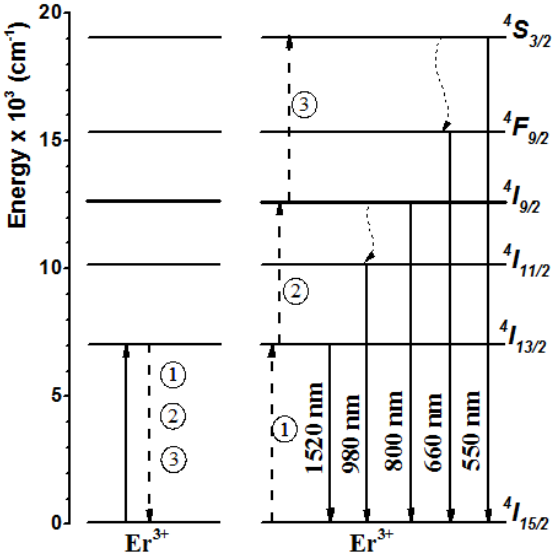

Another proof-of-principle is that when a luminescent layer is placed on the top level of a solar cell. Despite proved by Badescu, that first mentioned no benefits can be achieved by placing a UC material in front of a solar cell, studies have shown an

increase in the photocurrent when the samples are excited between 1480 and 1550 nm [RODRÍGUEZ-RODRÍGUEZ et al, 2016; KRISHNAIAH et al, 2017; HENKE et al, 2009]. Indeed, in a commercial point of view, a device in which a layer present deleterious effect to the global efficiency is not desired, otherwise merely for research and developing new luminescent materials. Moreover, since the layer do not modify the solar cell features but only the incident radiation by spectral modification, applications of layers on the top level of solar cell are still attractive to stud photocurrent enhancement by UC properties. Figure 1.12 shows three experimental setup to measure photocurrent response when a UC layer is placed on the top level of a silicon solar cell. In Figure 1.12a, a tellurite glass doped with Er^{3+} and excited at 1500 nm; in 1.12b, a fluoroindate glass co-doped with Yb^{3+}-Er^{3+} and is excited at 1480 nm and in 1.12c, Er^{3+} containing fluorozirconate glass is excited at 1540 nm. All the glasses are perpendicularly excited by a near-infrared source and the green color is due to the Er^{3+} transition ($^4S_{3/2} \rightarrow {}^4I_{15/2}$). In both cases, the samples are not use as encapsulated glass. In other words, samples are smaller than the active are of the solar cells, as we can see from the digital pictures (a), (b) and (c).

Figure 1.12. Working principle of a luminescent layer placed at the top level of a silicon solar cell. Adapted from the references [RODRÍGUEZ-RODRÍGUEZ et al, 2016; KRISHNAIAH et al, 2017; HENKE et al, 2009].

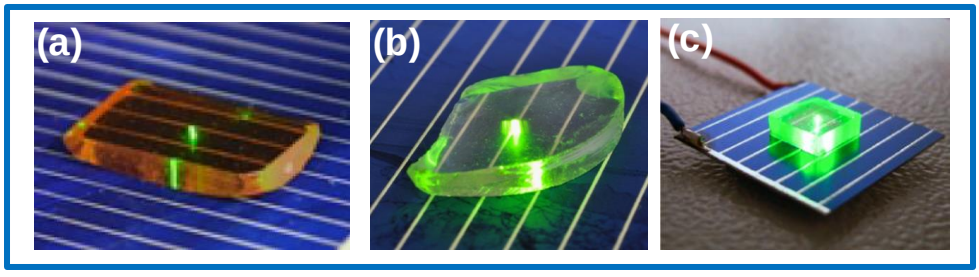

1.6 Materials for upconversion

There is a vast literature concerning monocrystalline and polycrystalline upconverter materials as luminescent layer for solar cell, in this section we introduced an overview regarding materials for potential upconversion application. Still, we restrict throughout the text to the use of the Er^{3+}-doped materials for UC in luminescent layers, as introduced in the last topics. As scribed before, lanthanide as Er^{3+}, for example, exhibit absorption in the near infrared. The main interest in materials for upconversion is that the window transparency extend to the visible and infrared domain [CALVEZ, 2017]. Visible transparency is defined by electronic transition from the valence band to the conduction band [NALIN et al, 2016]. In other words, the bandgap (Eg), that is the energy gap between the valence and conduction band, which is associated to short wavelengths, defines the transparency in the visible range. On the other hand, vibrational modes defines the transparency in longer wavelength (infrared). Generally, massive atoms such as selenium (Se), sulfur (S) and tellurium extend the transmission band to longer wavelengths [CALVEZ, 2017].

Figure 1.13 presents the window transparency for some Chalcogenide glasses. The global transparency is governed by the electronic transition (short wavelength) and vibrational modes (longer wavelength). Silica and fluoride glasses have high transparency in the visible range (not shown), meanwhile sulfides, selenides and tellurides glasses have lower transparency in the visible range.

Figure 1.13. Window transparency for Chalcogenide glasses [CALVEZ, 2017].

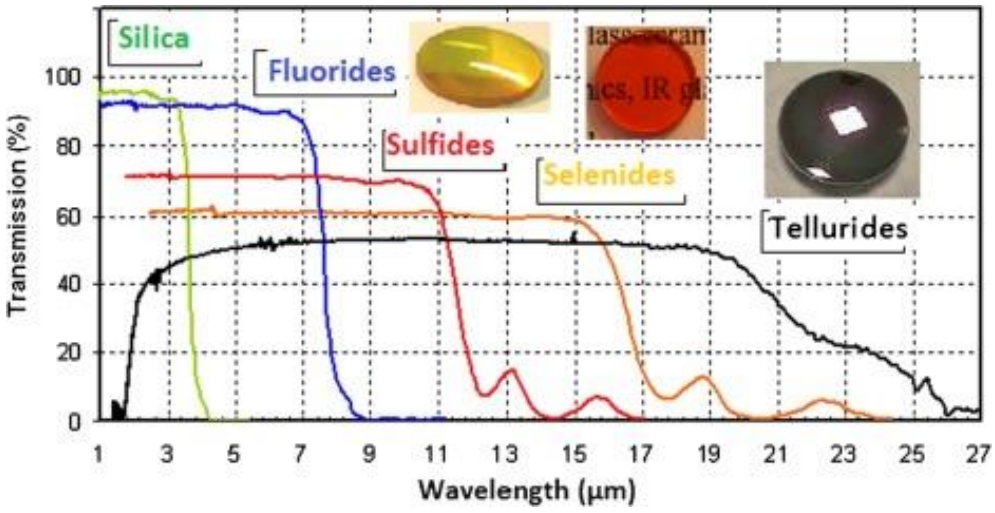

1.7 References

AHMED, M. I.; HABIB, A.; JAVAID, S. S. Perovskite Solar Cells: Potentials, Challenges, and Opportunities. **International Journal of Photoenergy.** v. 2015, pag. 1-13, 2015.

ANSPAUGH, B. E. GaAs Solar Cell Radiation Handbook. **JPL Publication**. pag. 1-63, 1996.

ASIM, N. et al. A review on the role of materials science in solar cells. **Renewable and Sustainable Energy Reviews.** v. 16, n. 8, pag. 5834-5847, 2012.

BADESCU, V. An extended model for upconversion in solar cells. **Journal of Applied Physics**, v. 104, n. 11, pag. 113120,1-113120-10, 2008.

BLOEMBERGEN, N. Solid State Infrared Quantum Counters. **Physical Review Letters**, v. 2, n. 3, pag. 84-85, 1959.

BUNZLI, J. and ELISEEVA, S. V. Lanthanide NIR luminescence for telecommunications, bioanalyses and solar energy conversion. **Journal of Rare Earths**. v. 28, n. 6, pag. 824-841, 2010.

BUNZLI, J. and PIGUET, C. Taking advantage of luminescent lanthanide ions. **Chemical Society Reviews**. v. 34, n. 12, pag. 1048-1077, 2005.

BUNZLI, J. et al. New Opportunities for Lanthanide Luminescence. **Journal of Rare Earths**. v. 25, n. 3, pag. 257-274, 2007.

CALVEZ, L. Chalcogenide glasses and glass-ceramics: Transparent materials in the infrared for dual applications. **Comptes Rendus Physique**. v. 18, n. 5-6, pag. 314-322, 2017.

CHEN, Z. et al. Highly efficient up-conversion luminescence in $BaCl_2$:Er^{3+} phosphors via simultaneous multiwavelength excitation. **Applied Physics Express**. v. 8, n. 3, 032301,1-032301,4, 2015.

CHOPRA, K. L.; PAUSON, P. D.; DUTTA, V. Thin-Film Solar Cells: An Overview. Progress in Photovoltaics: **Research and applications**. v. 12, pag. 69-92, 2004.

CORREIA et al. Luminescent solar concentrators: challenges for lanthanide-based organic–inorganic hybrid materials. **Journal of Materials Chemistry A**. v. 2, n. 16, pag. 5580-5596, 2014.

CUI, S. et al. From Selenium- to Tellurium-Based Glass Optical Fibers for Infrared Spectroscopies. **Molecules**. v. 18, pag. 5373-5388, 2013.

DONG, W. et al. Nanopatterned luminescent concentrators for visible light communications. **Optics Express**. v. 25, n. 18, pag. 21926-21934, 2017.

DWIVEDI, Y. and ZILIO, S. C. Advances in Rare Earth Spectroscopy and Applications. **Journal of Nanoscience and Nanotechnology**. v. 14, n. 2, pag. 1578-1596, 2013.

EICHELBAUM, M. and RADEMANN, K. Plasmonic Enhancement or Energy Transfer? On the Luminescence of Gold-, Silver-, and Lanthanide-Doped Silicate Glasses and Its Potential for Light-Emitting Devices. **Advanced Functional Materials**. v. 19, n. 13, pag. 2045-2052, 2009.

ELISEEVA, S. V. and BUNZLI, J. G. Lanthanide luminescence for functional materials and bio-sciences. **Chemical Society Reviews**. v. 39, pag. 189-227, 2010.

ELISEEVA, S. V. and BUNZLI, J. G. Rare earths: jewels for functional materials of the future. **New Journal of Chemistry**. v. 35, n. 6, pag. 1165-1176, 2011.

ENDE, B. V.; AARTS, L. and MEIJERINK, A. Lanthanide ions as spectral converters for solar cells. **Physical Chemistry Chemical Physics**. V. 11, n. 47, pag. 11081-11095, 2009.

GIBART, P. et al. Below Band-gap IR Response of Substrate-Free GaAs Solar Cells Using Two-Photon Up-conversion. **Journal of Applied Physics**. v. 35, pag. 4401-4402, 1996.

GREEN, M. A. et al. Solar cell efficiency tables (Version 45). **Progress in Photovoltaics: Research and Applications**. v. 23, n. 7, pag. 1-9, 2015.

GREEN, M. A. Third generation photovoltaics: solar cells for 2020 and beyond. **Physica E: Low-dimensional Systems and Nanostructures**. v. 14, n. 1-2, pag. 65-70, 2002.

GOETZBERGER, A.; HEBLING, C.; SHOCK, H. W. Photovoltaic materials, history, status and outlook. **Materials Science and Engineering R**. v. 40, pag. 1-46, 2003.

GOLDSCHMIDT, J. C. and FISHCER, S. Upconversion for Photovoltaics – a Review of Materials, Devices and Concepts for Performance Enhancement. **Advanced Optical Materials**. v. 3, n. 4, pag. 510-535, 2015.

HAMANN, T. W. et al. Advancing beyond current generation dye-sensitized solar cells. **Energy & Environmental Science**. n. 1, pag. 66-78, 2008.

HENKE, B. et al. Upconverting glasses for high-efficiency solar cells. **SPIE**. pag. 1-3, 2009.

JACOBSON, M. and DELUCCHI, M. A. Providing all global energy with wind, water, and solar power, Part I: Technologies, energy resources, quantities and areas of infrastructure, and materials. **Energy Policy**. v. 39, n. 3, pag. 1154-1169, 2011.

JEAN, J. et al. Pathways for solar photovoltaics. **Energy & Environmental Science**. v. 8, n. 4, pag. 1200-1219, 2015.

JORGENSEN, C. K. and REISFELD, R. Chemistry and Spectroscopy of Rare Earths. **Springer Link**. v. 100, pag. 127-167, 2008.

JOUBERT, M. Photon avalanche upconversion in rare earth laser materials. **Optical Materials**. v. 11, n. 2, pag. 181-203, 1999.

KANG, M. et al. Toward Low-Cost, High-Efficiency, and Scalable Organic Solar Cells with Transparent Metal Electrode and Improved Domain Morphology. **IEEE Journal of Selected Topics in Quantum Electronics**. v. 16, n. 6, pag. 1-14, 2010.

KARATAIRI, E. and HOPPE, H. Are rare earths part of a bright future for lighting and displays?. **Materials Research Bulletin**. v. 41, pag. 432, 2016.

KRISHNAIAH, K. V. et al. Er^{3+}-doped tellurite glasses for enhancing a solar cell photocurrent through photon upconversion upon 1500nm excitation. **Materials Chemistry and Physics**. v. 199, pag. 67-72, 2017.

LALLA, E. A. et al. Optical temperature sensor based on the Nd^{3+} infrared thermalized emissions in a fluorotellurite glass. **Journal of Luminescence**. v. 166, pag. 209-214, 2015.

LIAN, H. et al. Rare earth ions doped phosphors for improving efficiencies of solar Cells. **Energy**. v. 57, n. 1, pag. 270-283, 2013.

LIU, C.; HOU, Y.; and GAO, M. Are Rare-Earth Nanoparticles Suitable for In Vivo Applications?. **Advanced Materials**. v. 26, n. 40, pag. 6922-6932, 2014.

LUNT, R. R. and BULOVIC, V. Transparent, near-infrared organic photovoltaic solar cells for window and energy-scavenging applications. **Applied Physics Letters**. v. 98, pag. 113303,1-113303,3, 2011.

NALIN, et al. Materiais vítreos e luz: Parte 1. **Química Nova**, 2016.

QIAO, Y, et al. Recent Advances of Rare-Earth Ion Doped Luminescent nanomaterials in Perovskite Solar Cells. **Nanomaterials**. v. 8, n. 43, pag. 1-11, 2018.

REID, M. F. Theory of Rare-Earth Electronic Structure and Spectroscopy. **Handbook on the Physics and Chemistry of Rare Earths.** v. 50**,** pag. 47-64, 2016.

RICHARDS, et al. Enhancing the performance of silicon solar cells via the application of passive luminescence conversion layers. **Solar Energy Materials & Solar Cells**. v. 90, n. 15, pag. 2329-2337, 2006.

RODRÍGUEZ-RODRÍGUEZ, H. et al. Analysis of the upconversion process inTm^{+3} doped glasses for enhancement of the photocurrent in silicon solar cells. **Solar Energy Materials & Solar Cells**. v. 144, pag. 29-32, 2016.

RODRÍGUEZ-RODRÍGUEZ, H. Experimental enhancement of the photocurrent in a solar cell using upconversion process in fluoroindateglassesexcitingat1480nm. **Solar Energy Materials & Solar Cells.** v. 116, pag. 171-175, 2013.

RUHLE, S.; SHALOM, M.; ZABAN, A. Quantum-Dot-Sensitized Solar Cells. **ChemPhysChem**. v. 11, pag. 2290-2304, 2010.

SARK, W. G. J. H. M.; MEIJERINK, A. and SCHROPP, R. E. I. Solar Spectrum Conversion for Photovoltaics Using Nanoparticles. **Third Generation Photovoltaics**. InTech, 2012.

SHALAV, A.; RICHARDS, B. S. and GREEN, M. A. Luminescent layers for enhanced silicon solar cell performance: Up-conversion. **Solar Energy Materials & Solar Cells.** v. 91, n. 9, pag. 829-842, 2007.

SCHOCKLEY, W. and QUEISSER, H. Detailed Balance Limit of Efficiency of pn Junction Solar Cells. **Journal of Applied Physics**. v. 32, n. 3, pag. 510-519, 1961.

SCHWEIZER, S. et al. Down-Conversion in Rare-Earth Doped Glasses and Glass Ceramics. **Wiley-VCH Verlag**, 2015.

SHPAISMAN, H. et al. Can up- and down-conversion and multi-exciton generation improve photovoltaics? **Solar Energy Materials & Solar Cells**. v. 92, n. 12, pag. 1541-1546, 2008.

SOLÉ, J. G.; BAUSÁ, L. E. and JAQUE, D. An Introduction to the Optical Spectroscopy of Inorganic Solids. **John Wiley & Sons, Ltd**, 2005.

SONG, P.; ZHANG, C. and ZHU, P. Enhanced solar photons harvesting of a-Si:H solar cells with ZBLA fluoride glasses containing rare earth ions. **Journal of Alloys and Compounds**. v. 678, pag. 65-69, 2016.

SONG, P.; ZHANG, C. and ZHU, P. Eu^{3+}-Mn^{2+}-doped bi-functional glasses with solar photon downshifting: Application to CdS/CdTe solar cells. **Journal of Alloys and Compounds**. v. 661, n. 15, pag. 14-19, 2016.

SUN, L. et al. Upconversion of Rare Earth Nanomaterials. **Annual Review**. v. 63, pag. 619-642, 2015.

STEUDEL, F.; DYRBA, M. and SCHWEIZER, S. Fluorescent borate glass enhances cadmium telluride solar cells. **Spie**. v. 8438, pag. 1-2, 2012.

STRUMPEL, et al. Modifying the solar spectrum to enhance silicon solar cell efficiency – An overview of available materials. **Solar Energy Materials & Solar Cells**. v. 91, n. 4, pag. 238-249, 2007.

TANABE, S. Glass and Rare-Earth Elements: A Personal Perspective**. International Journal of Applied Glass Science**. v. 6, n. 4, pag. 305-328, 2015.

TRUPKE, T.; GREEN, M. A. and WURFEL, P. Improving solar cell efficiencies by up-conversion of sub-band-gap light. **Journal of Applied Physics**. v. 92, n. 7, pag. 4117-4122, 2002.

TRUPKE, T.; GREEN, M. A. and WURFEL, P. Improving solar cell efficiencies by down-conversion of high-energy photons. **Journal of Applied Physics**. v. 92, n. 3, pag. 1668-1674, 2002.

ULLAH, S. et al. Microwave-assisted synthesis of NaYF4:Yb^{3+}/Tm^{3+} upconversion particles with tailored morphology and phase for the design of UV/NIR-active $NaYF_4$:Yb^{3+}/Tm^{3+}@TiO_2 core@shell photocatalysts. **CrystEngComm**. v.19, n. 25, pag. 3465-3475, 2017.

VASILIEV, M. et al. Photonic microstructures for energy-generating clear glass and net-zero energy buildings. **Scientific Reports**. v. 6, n. 31831, pag. 1-14, 2016.

VERGEER, P. et al. Quantum cutting by cooperative energy transfer in $Yb_xY_{1-x}PO_4$:Tb^{3+}. **Physical Review B**. v. 71, n. 1, pag. 014119,1-014119,11, 2005.

WANG, F. et al. Tuning upconversion through energy migration in core–shell nanoparticles. **Nature Materials**. v. 10, pag. 968-973, 2011.

WANG, K. et al. Upconversion enhancement of lanthanide-doped $NaYF_4$ for quantum dot-sensitized solar cells. **Electrochimica Acta**. v. 155, n. 10, pag. 357-363, 2015.

WHEG, R. T. et al. Extending Dieke's diagram. **Journal of Luminescence**. v. 87-89, pag. 1002-1004, 2000.

WYBOURNE, B. G. The fascination of the rare earths: then, now and in the future. **Journal of Alloys and Compounds**. v. 380, pag. 96-100, 2004.

YUHUA, W. et al. Recent development in rare earth doped phosphors for white light emitting diodes. **Journal of Rare Earths**. v. 33, n. 1, pag. 1-12, 2015.

General Conclusions

Fluoroindate and fluorophosphate glasses were prepared through the melting-quenching method. These two family of glasses were selected according to the physics and chemical properties. The low energy phonon matrix (fluoroindate) yielded a very intense upconversion emission for the sample with 7 mol% of Er^{3+}, in consequence, a high photocurrent was observed for low power excitation (22 mW). However, due to the low absorption and emission coefficient of the lanthanides, it is still far the application in spectral converters to increase solar cells efficiency. From the fluorophosphate glasses results, we conclude a size-dependence for the Ag NC's stabilization. The F^- ions played an important role on the Ag NC's reduction. In addition, the long molecular weight introduced by the metaphosphate groups may be a crucial reason for a non-agglomeration of Ag ions, since the phosphate groups may leave voids in the glass network. However, this is still in investigation in our research group. The dispersion of 5 mol% of Ag, seems to be an ideal concentration for Ag NC's obtention and SPR-free samples. This sample with 5 mol% showed a broadband emission that started in the UV region and extended until infrared at 730 nm. This broadband resulted from a size-distribution behavior in which the formation of nanoclusters responsible for the blue, green and red emission is observed. Still, silver nanoclusters showed an energy transfer (ET) to the rare-earths Pr^{3+} and Yb^{3+}. The composition with less amount of metaphosphate groups, allowed to disperse a less amount of silver, in consequence, 2 mol% was the optimum concentration to avoid the obtention of opaque glasses with SPR effect, as it was obtained for 4 and 10 mol%. However, the samples even for high amount present broadband emission in the visible range. For the last, very bright microstructures of silver were obtained after interaction of the sample with 5 mol% and the femtosecond laser. This sample showed to be a good candidate for waveguide application.